Journal of Electroanalytical Chemistry 896 (2021) 115222

Contents lists available at ScienceDirect

Journal of Electroanalytical Chemistry

journal homepage: www.elsevier.com/locate/jelechem

Cement mortar cracking under accelerated steel corrosion test: A mechanical and electrochemical model

E.G. Segovia [a], G. de Vera [a,*], M. Miró [a], J. Ramis [b], M.A. Climent [a]

[a] Civil Engineering Department, University of Alicante, PO Box 99, 03080 Alicante, Spain
[b] DFISTS, University of Alicante, PO Box 99, 03080 Alicante, Spain

ARTICLE INFO

Keywords:
Cracking
Non-uniform corrosion
Corrosion test
Mechanical model
Electrochemical model
Mortar

ABSTRACT

Corrosion of the embedded steel is one of the main degradation problems limiting the service life of reinforced and pre-stressed concrete structures. A model able to provide approximate predictions of the evolution of the cracking process can be useful for designing accelerated corrosion tests of reinforced cement mortar or concrete specimens. An electrochemical model has been used for describing the inner displacements and strains caused by the accumulation of steel corrosion products around the rebar during electrically accelerated corrosion tests of reinforced cement mortar specimens with simple geometries. Subsequently, a mechanical model using the XFEM-Based Crack Growth Simulation module of Ansys Software, has been implemented to describe the distribution of stresses in the cross-section of the specimens. The combined electrochemical and mechanical model has led to acceptable predictions of the time to appearance of the first surface crack and the evolution of crack width over time. This combined model, which needs only data of a few experimental parameters, and uses only readily accessible standard software, could easily be implemented with other experimental configurations. For a more realistic description of the distribution of the tensile stresses and of the whole cracking process, the model must consider the initiation of several cracks, at least eight, around the rebar perimeter. The inclusion in the model of higher number of cracks increases greatly the computation time and effort, and may lead to convergence difficulties.

1. Introduction

Corrosion of the embedded steel is one of the main degradation problems limiting the service life of reinforced and pre-stressed concrete structures, both in buildings and civil infrastructure [1]. The process starts with depassivation of steel, usually triggered by carbonation [2] or chloride contamination of concrete [3]. Afterwards, the steel corrosion rate depends on the environmental conditions, mainly on the humidity of concrete and on the access of oxygen. Corrosion converts progressively the steel rebar into oxides which have a higher volume (2 to 6 times) than the metal. A significant part of the corrosion products continuously accumulate remaining as a solid layer around the rebar [4]. This is why, from a mechanical point of view, the expansion associated with the formation of steel corrosion products can be interpreted as a rebar volume increase, which generates internal tensile stresses. However, it is known that in certain circumstances, especially in very humid concrete, some of the corrosion products can be transported away from the rebar [5], thus partially alleviating the tensile stresses around the rebar. Eventually, the tensile stresses can overcome the tensile strength of concrete, leading to micro and macro cracking of the cementitious composite [6,7], and being at the origin of the damage suffered by concrete [4]. Further consequences of the corrosion of embedded steel are the spalling or delamination of the concrete cover, loss of bond between concrete and steel, loss of steel ductility, and loss of cross-sectional area of steel, so the structure's strength weakens [8]. These phenomena contribute to reducing the serviceability and load bearing capacity of the structures. Another aspect which needs to be taken into account is that the cracks of the concrete cover over steel represent a preferential path of enhanced ingress of deleterious substances into concrete, such are the chloride ions. Hence cracking can contribute to further increase the corrosion rate of steel reinforcements. Usually, cracking of the concrete cover is considered as the event indicating the end of the service life of concrete structures affected by steel reinforcement corrosion [9,10]. Thus, great effort has been devoted to studying the cracking of concrete due to corrosion of the embedded steel rebar [11–18].

* Corresponding author.
E-mail address: guillem.vera@ua.es (G. de Vera).

https://doi.org/10.1016/j.jelechem.2021.115222
Received 23 December 2020; Received in revised form 25 March 2021; Accepted 28 March 2021

Cracking of concrete due to embedded steel corrosion has been experimentally studied through accelerated corrosion tests [5–7,12,15,19–22], which use an external electric field and high corrosion rate values (typically $100\mu A/cm^2$ or higher). The classical experimental studies are usually based on the microscopic observation of the appearance of the first surface crack and the recording of the crack width growth with time. This allows establishing a relation between crack width and corrosion level in terms of the corrosion penetration depth. Main results indicate that concrete cracking consists of two steps: generation of the cracks and propagation. Andrade et al. [12] indicated that only a few micrometers of loss in steel rebar radius due to corrosion are needed to induce visible concrete cover cracks (0.05–0.1 mm width), under accelerated corrosion tests. Alonso et al. [6] found a linear relationship between the amount of steel corrosion penetration (or time) and concrete crack width during the propagation step. However, these classical experimental studies do not provide information regarding the cracking generation period. Only very recently the X-ray microcomputed tomography technique has allowed obtaining three-dimensional images of the morphology of the microcracking of concrete during the early stages of embedded steel corrosion [21].

Due to the high economic and social costs associated to the degradation of concrete structures by steel reinforcement corrosion, much effort has been dedicated to developing non-destructive techniques (NDT) for assessing the corrosion state and the damage level, especially at the early stages of the process, when the symptoms are still not visible. It is widely accepted that the costs of rehabilitation are highly reduced if decisions on prevention or reparation can be promptly taken. The classical electrochemical techniques, such as corrosion potential, electrical resistivity of concrete and corrosion rate, allow easy detection of the risk and activity of the corrosion process [23–28]. Especial mention deserves the measurement of the steel corrosion rate through techniques like the polarization resistance method [27,28], which provide essential data for the mathematical models allowing estimations of the remaining service life of the structures [10]. However, the electrochemical techniques do not inform on the concrete damage, i.e. they are insensitive to the presence or absence of microcracking of the concrete cover. Other techniques based on propagation of elastic waves [29–31], like ultrasounds, have been recently shown to be useful for detecting damage and defects in materials, like microcracking. For instance Acoustic Emission [32–34], Impact-Echo [35], and Non-Linear Ultrasonic (NLU) techniques [36–38] have been used to detect cracks in early stages. These are indirect techniques which need calibration against experimental observations and experimental data. Modelization of the cracking process may be helpful in research devoted to developing NDT for assessing the concrete damage. For instance, some capability of prediction of the time of appearance of the surface cracks is needed for adequately designing the protocols and the values of the relevant experimental parameters in the accelerated corrosion tests.

Rigorous mathematical modelization of the concrete cover cracking due to embedded steel corrosion is highly challenging due to the complexity of the involved physico-chemical processes. It is first needed an electrochemical model providing information about the formation of steel corrosion products, including its spatial distribution around the rebar, and its evolution. In second place the outcomes of the electrochemical model must be fed into a mechanical model in order to calculate the tensile stresses generated in the cementitious matrix and its eventual overcoming of the tensile strength of concrete. Certain detailed models [13,14,39], developed for situations where reinforced concrete is exposed to a chloride laden environment, include a chloride transport model through concrete in order to describe also the stage previous to the depassivation of steel (building of a high enough chloride content in the concrete layers in contact with steel), thus allowing to estimate also the time of initiation of corrosion.

Some models consider uniform corrosion along the rebar perimeter [39,40], although corrosion is frequently localized (chlorides are known to promote pitting corrosion). Furthermore in the case of complex structures the corrosion process might be highly non-uniform due to situations like the presence of galvanic macrocouples [8]. Considerable effort has been devoted to develop models able to take into account the non-uniform character of the corrosion process in many situations [13,14,16–18,41–46]. In cases where corrosion is due to chloride ions ingressed into concrete from the environment, the rebar shape is considered to evolve to an ellipsoid [14,16,17,42] as the corrosion propagates and the outer layer of the steel bar is converted into oxides. Different geometries, combination of ellipsoids [19] and others [15,41], have been considered. In the case of accelerated corrosion tests, the use of an electric field with a simple geometry allows relatively easier calculations of the current density distribution along the rebar perimeter.

Regarding the mechanical models, a large number of numerical models have been developed. Back in 2013, Jamali et al. [11] made a critical analysis on modeling of corrosion-induced concrete cover cracking, studying a number of empirical, analytical and numerical models to predict the time to cracking, and it was observed that the majority of the investigation models were only capable of adequately predicting the time-to-cracking for the experiments to which they were fitted. Later, more complex mechanical models have been developed; all implemented models use numerical methods for concrete cracking caused by non-uniform corrosion, such as the finite element model (FEM), two-dimensional lattice model, rigid body spring model (RBSM), boundary element method, and so on [11,13,14,16–18,41,42], always trying to improve predictions. However, practically all of the detailed models developed for describing the evolution of the corrosion induced cracking of concrete use on-purpose developed software which is not accessible to other researchers and laboratories.

This work is part of a project aimed at demonstrating the utility of NLU techniques for the early detection of cement mortar cracking due to embedded steel corrosion [47,48]. The specific objective of the research reported here has been to develop a resort model able to provide approximate predictions of the evolution of the cracking process, in order to facilitate the design of the experiments of accelerated corrosion of reinforced cement mortar specimens (duration of the experiments and selection of the relevant experimental parameters like the anodic current density). An electrochemical model has been used for describing the evolution of the rebar shape due to the accumulation of corrosion products generated during the electrically accelerated corrosion test [49]. Subsequently, a mechanical model has been implemented based on the standard use of Ansys Software [50] and the eXtended Finite Element Model (XFEM) [51], reaching an acceptable prediction of the time to appearance of the crack on the surface and the evolution of the width of the crack over time using standard software, which could easily be implemented to perform modeling of other specimen configurations.

2. Materials and methods

Testing was conducted on reinforced cement mortar elements. The specimens were of prismatic shape, with a single steel rebar as the reinforcement. The choice of using cement mortar instead of concrete was due to the interest in using a more homogeneous and simpler model material, by avoiding the presence of coarse aggregate, which could create heterogeneities at the steel–concrete interface. The corrosion of steel was forced by the application of an electric field, between the steel rebar (anode), and an external cathode [47].

2.1. Preparation of the Reinforced Cement Mortar Specimens

The cement mortar was prepared with a sulfate-resisting ordinary Portland cement, CEM I 52,5 R SR(3), following the European standard [52]. The aggregate was standard siliceous sand. The water-cement ratio (w/c) of the mortar was 0.5, and sodium chloride was dissolved into the mixing water to obtain a content of 2% Cl^- relative to the cement weight in the hardened mortar [53]. Samples were manually compacted. The composition details are given in Table 1. Mortar compressive strength was measured on eight samples according to standard [54], resulting a mean value of 29 MPa (1.6 MPa standard deviation) after seven days of curing. Mortar density was measured on four samples according to standard [55], resulting a mean value of 2000 kg/m^3 (20 kg/m^3 standard deviation).

Two series (A and B) of prismatic mortar specimens were tested. Geometrical details of the specimens are summarized in Table 2. Wooden molds were used for series A and plastic ones were used for series B. A single steel rebar (deformed surface in series A and smooth surface in series B) with 12 mm diameter was embedded in the specimens. Rebar was located in one of the main symmetry planes of the specimen. Before putting the steel bar into the empty mold, the steel surface was cleaned from the native corrosion products, following a recommended procedure [56]. The ends of the steel bar were protected with vinyl electric tape, to avoid the triple contact steel-mortar-air, leaving an exposed steel area of 120 cm^2 (the steel-mortar surface of contact). The mortar specimens were compacted manually, finished, and left in the molds over 24 h. After demolding, the specimens were cured over seven days in a humid chamber (20 °C and 95% relative humidity).

2.2. Corrosion test

The forced corrosion tests were performed by applying an electrical field between the steel rebar (anode) and an external cathode, consisting of a galvanized steel grid. The tests were run during 23 days in galvanostatic conditions (a constant anodic current density of $100\mu A/cm^2$), using an electrophoretic power source. During the tests, the bottom of the mortar specimens was kept in permanent contact with tap water (the maximum height of the contact between water and mortar is 5 mm), in order to maintain an adequate level of electric conductivity for the material. The mortar specimen was put on top of the cathode, with a polypropylene sponge in between them as shown in Fig. 1.

2.3. Microscopic inspection

Due to the chosen setup and geometric conditions of the experiments, the cracks due to steel corrosion appeared at the upper surface of the mortar specimens. This fact allowed the detection of the appearance of cracking and an easy periodic inspection of this surface with a crack width microscope (magnification 40X, model 58-C0218, Controls, Milan, Italy). In this way, it was possible to detect the appearance of the first surface micro-crack, and the posterior monitoring of the growth of the crack width with time.

Table 1
Mortar composition.

Material	Amount (g)
Cement (CEM I 52,5 R SR(3))	450
Standard siliceous sand	1350
Deionized water	225
NaCl	14.8

Table 2
Geometrical details of mortar specimens.

Series	Dimensions (cm)	Concrete cover depth over steel (mm)	Rebar diameter Ø (mm)
A	8 × 8 × 35	10	12
B	10 × 10 × 35	25	12

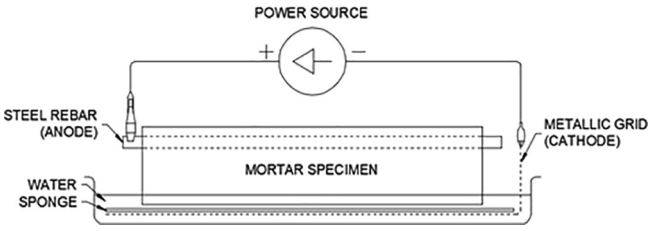

Fig. 1. Corrosion test.

3. Cracking model

An electrochemical model was previously developed [49] to obtain rebar shape evolution during the performed corrosion test. It is here outlined. Rebar metal loss is considered to be due to the anodic impressed current. Current density along rebar perimeter is calculated solving the appropriate differential equation. The obtained current density is not uniform along the rebar perimeter. Faraday's law is then used to relate current density with volume of metal lost. As current density is not uniform, metal loss is also not uniform along rebar perimeter, and so the bar loses its initial circular shape. The dissolved metal is assumed to react to form solid corrosion products that are bulkier than the original metal. It is assumed that solid corrosion products stay where they are formed, laying a solid layer of corrosion products around the metallic rebar. The thickness of this layer is also not uniform along the rebar perimeter. As a result, in comparison with the original circular section of diameter D, it is obtained a narrower non-circular metal section of radius $r_m(\theta,t)$ covered by a non-uniform layer of corrosion products, that yield as a whole a thicker non-circular bar of radius $r_{ox}(\theta,t)$. The bar will result thicker where the current density is higher. This expanded bar is considered as the cause of mortar cracking. The electrochemical model is solved in terms of the current function Ψ whose level curves are the current streamlines. Laplace equation must be solved:

$$\frac{\partial^2\Psi}{\partial x^2}+\frac{\partial^2\Psi}{\partial y^2}=0 \tag{1}$$

This equation is solved using an standard FEM method. Current density along rebar perimeter is then calculated as:

$$j(\theta,t)=\frac{1}{r_m(\theta,t)}\cdot\frac{\partial\Psi(\theta,t)}{\partial\theta} \tag{2}$$

where t is time and θ is counterclockwise angle in degrees from top of rebar. This expression and Faraday's Law are used in each time step to recompute metal radius as:

$$r_m(\theta,t)=\frac{D}{2}-\frac{M}{nF\rho}\int_0^t j(\theta,t)dt \tag{3}$$

where $M=55.85\ g/mol$ is the metal molar mass, $n=2$ is the number of electrons in the oxidation reaction, $F=96485\ C/mol$ is the Faraday's constant, and $\rho=7850\ kg/m^3$ is the metal density.

A remeshing is needed after each time step due to the rebar shape change. The radius of the whole bar, including oxides layer, is calculated as:

$$r_{ox}(\theta,t)=\sqrt{\frac{D^2}{4}+(\alpha-1)\left(\frac{D^2}{4}-r_m^2(\theta,t)\right)} \tag{4}$$

where $\alpha=2$ [57] is the ratio of oxides volume to metal volume. Here it is assumed that the formed oxides stay around the rebar creating a layer between the metal and the mortar. This layer is bulkier then the original metal, provoking a displacement of the mortar [49]. The resulting $r_{ox}(\theta,t)$ is used as input in the mechanical crack model described below.

Mechanical model was implemented using Ansys Software [50]. XFEM-Based Crack-Growth Simulation was used. The *eXtended Finite Element Method (XFEM)*, introduced by Belytschko and Black [51], models cracks and other discontinuities by enriching the degrees of freedom in the model with additional displacement functions that account for the jump in displacements across the discontinuity and so overcomes the requirements of updating the mesh as the crack grows. XFEM is based on the partition of unity concepts, first outlined by Melenk and Babuska [58–61]. Phantom-Node Method was used. A crack-growth criterion must be specified for newly cracked cohesive segments to initiate ahead of the existing cracks. When the critical value of the crack-growth criterion is reached ahead of the crack, new cohesive segments are introduced in the elements ahead of the current crack front. The crack-growth criteria is maximum circumferential stress criterion [62]. When the cohesive segments are initiated, the cohesive stresses in the crack segments gradually decrease to zero as the deformation progresses. The decay of the cohesive stresses is modeled based on a rigid linear cohesive law [63]. Mode I fracture was considered, and the needed material parameters were estimated, according to CEB/FIP Model Code [64], from measured mean compressive strength ($f_{cm}=29\,MPa$). Tangent modulus of elasticity E_c is given by:

$$E_c=0.85\cdot\alpha_E\cdot 2.15\cdot 10^4 MPa\cdot\left(\frac{f_{cm}}{10MPa}\right)^{1/3} \tag{5}$$

where α_E is related with type of aggregate. The value $\alpha_E=1.0$ for quartzitic aggregate has been used. The factor 0.85 in Eq. (5) accounts for the initial plastics strains. Mean axial tensile strength f_{ctm} is given by:

$$f_{ctm}=2.12\,MPa\cdot\ln\left(1+\frac{f_{cm}}{10\,MPa}\right) \tag{6}$$

Fracture energy G_F is given by:

$$G_F=G_{F_0}\left(\frac{f_{cm}}{10\,MPa}\right)^{0.7}\qquad(f_{cm}\le 80\,MPa) \tag{7}$$

where G_{F_0} is the base value of fracture energy which depends on maximum aggregate size d_{max} as given in Table 3 (Tables 3.1–3 in Ref. [64]). The value $G_{F_0}=0.025\,N/mm$ has been extrapolated and used for $d_{max}=4\,mm$ from Table 3. This extrapolation seems to be reasonable according to the low variation of G_{F_0} in the range $8\,mm<d_{max}<16\,mm$. Crack opening when tensile-stress is zero σ_{max} is given by:

$$\sigma_{max}=\frac{2G_F}{f_{ctm}} \tag{8}$$

where a triangular diagram of tensile-stress vs. crack opening has been considered. The value used for de Poisson coefficient ($\nu=0.2$) is the value prescribed by the Spanish code for structural concrete [10] (chapter 8, paragraph 39.9). This value applies for concrete, but similar values have been experimentally found for cement mortar [65]. Used parameters are shown in Table 4.

Geometry of the used models is shown in Fig. 2 where plane deformation (infinite length assumed) is used. Eight initially closed cracks are considered and their locations and numbering are also shown in Fig. 2. One area is reserved for each crack propagation (areas A to H in Fig. 2 reserved for cracks 1 to 8 respectively). Cracks propagate normal to rebar perimeter. Three cases were studied: (i) only one crack (number 1 and area A in Fig. 2), (ii) four cracks (numbers 1, 3, 5, and 7, and areas A, C, E, and G respectively in Fig. 2) and (iii) eight cracks (numbers 1 to 8 and areas A to H respectively in Fig. 2). Each case uses approximately 71500 nodes and 71000 elements. All used elements are PLANE182 type (plane deformation, full integration with B method and pure displacement formulation) [50].

Load has been introduced as a radial displacement applied on the rebar perimeter. This displacement has been numerically obtained through the above mentioned electrochemical model. In order to get an analytical function, data have been fitted using non-linear least squares method to the following functions:

$$\begin{aligned} u_r&=\tfrac{t}{50}(0.156906-0.0801103\cos\theta)\quad(Series\,A)\\ u_r&=\tfrac{t}{50}(0.157077-0.0578407\cos\theta)\quad(Series\,B)\end{aligned} \tag{9}$$

Where time t is expressed in days, θ in degrees, and the displacement u_r is obtained in *mm*. Maximum fitting error was lower than 5%.

4. Results and discussion

Experimental crack width evolution with time is shown in Fig. 3 for series A (5 specimens) and in Fig. 4 for series B (6 specimens; 3 crack locations (labeled as B6a, B6b, and B6c) were measured on specimen B6). A first stage of the corrosion process seems to exist, during which there is no visible crack. This would be the generation step following Andrade and co-workers [6,12,22,57]. Afterwards, the crack width shows an approximately linear increase with time. This would be the propagation step [6,12,22,57]. Linear fit of the experimental data for the propagation step yields the following expressions:

$$\begin{aligned} Series\,A:&\quad w=-39.67+12.24t\quad(r=0.9346)\\ Series\,B:&\quad w=-71.13+14.56t\quad(r=0.9310)\end{aligned} \tag{10}$$

where t is time in days and w is crack width in μm. According to the linear fit, first crack appears at 3.2 days for series A and at 4.9 days for series B. These results are in agreement with the findings of previous authors [6]. Alonso et al. conducted accelerated corrosion tests on reinforced concrete specimens, similar to those described here [6]. These authors proposed an empiric linear relationship between the steel corrosion penetration able to produce a first crack at the concrete surface, and the ratio between the concrete cover depth and the rebar diameter ($c/\varnothing$). The corrosion penetration is expressed as the metallic bar radius reduction (x_0 in μm) needed to produce a visible crack at the concrete surface (crack width of $0.050mm$).

$$x_0=7.53+9.32\frac{c}{\varnothing}\quad\left(2<\frac{c}{\varnothing}<3\right) \tag{11}$$

Table 3
Base value of fracture energy.

Maximum aggregate size d_{max} (mm)	Base value of fracture energy G_{F_0} (N/mm)
8	0.025
16	0.03
32	0.058

Table 4
Parameters of the cement mortar used in the mechanical model.

Parameter	Value
Tangent modulus of elasticity E_c	26061 MPa
Mean axial tensile strength f_{ctm}	2.885 MPa
Fracture energy G_F	52.677 N/m
Crack opening when tensile-stress is zero σ_{max}	0.0365 mm
Density	2000 kg/m^3
Poisson coefficient	0.2

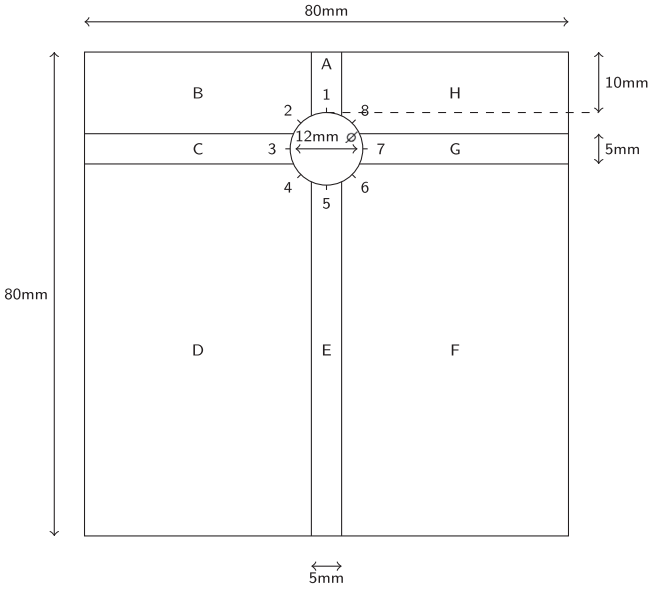

Fig. 2. Mechanical model geometry for the 8 $cm \times 8\ cm \times 35\ cm$ specimen. Cracks are marked with numbers, and their expansion zones are marked with capital letters.

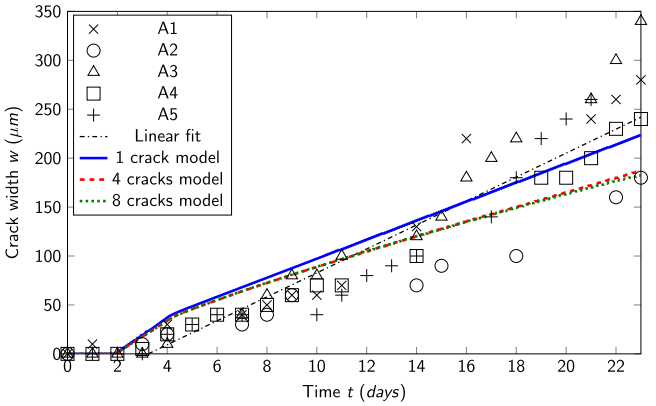

Fig. 3. Experimental and calculated crack width. Series A.

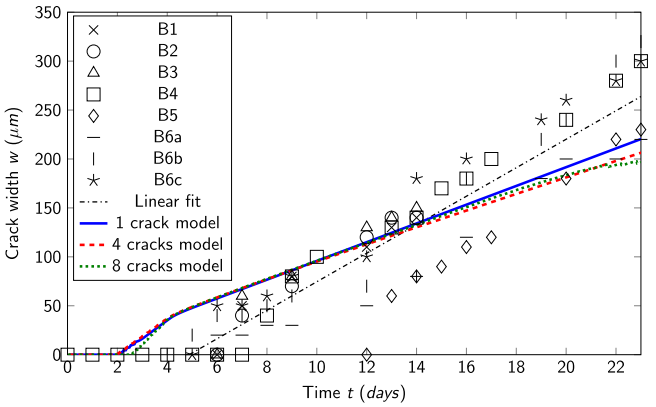

Fig. 4. Experimental and calculated crack width. Series B.

where Alonso assumes homogeneous rebar corrosion (circular rebar shape). Then, metal radius reduction relates to time through Faraday's law as:

$$x = 0.0319 I_{corr} t \tag{12}$$

With applied current I_{corr} in $\mu A/cm^2$, t in days, and x in μm. Thus, cover to rebar diameter ratio can be related with time for 50 μm crack width ($t_{50\ \mu m}$ in days) as:

$$t_{50\ \mu m} = \frac{1}{I_{corr}} \left(236.05 + 292.16 \frac{c}{\varnothing} \right) \quad \left(2 < \frac{c}{\varnothing} < 3 \right) \tag{13}$$

This expression yields 4.8 days and 8.4 days for series A and series B respectively, which compares to values 7.3 days and 8.3 days respectively obtained from linear fit Eq. (10). Series B is in good agreement with Eq. (13). For series A the agreement is not so good, but it should be kept in mind that its $\frac{c}{\varnothing}$ ratio (0.83) is below the application range of Eq. (13) (between 2 and 3).

The application of the mechanical model shows that the introduced energy is released more easily by opening the odd-numbered cracks than the even-numbered ones (see Fig. 2). It is also observed that crack 1 is the easiest to open. So crack 1 is the most important one to be considered. The importance of crack 1 is also put in evidence by the fact that the model calculations indicate that it reaches the concrete surface after 1.95 days, while the other cracks do not reach the surface in the studied period.

The calculated crack widths of crack 1 using the mechanical models with 1, 4, and 8 cracks are also shown in Figs. 3 and 4 for series A and B, respectively. Taking into account the high scatter of the experimental data, the agreement of the calculated values with the experimental ones is reasonably good. A better agreement is found for series A.

Time to appearance of first crack on the surface according to mechanical models (about 2 days) is in reasonable agreement with experimental fit for series A (3.2 days, Fig. 3). The agreement is not so good for series B (Fig. 4). This could be due to the different geometry of the mortar specimens in series A and B. A bigger specimen cross section and a higher concrete cover depth over steel provide a bulkier environment around the rebar in the case of series B. A more even distribution of energy among the existing cracks is expected for series B, thus slowing down the width growth of crack 1 as compared to series A. In support of this idea is the fact that the first appearance of a surface crack according to the 8 cracks model occurs later (at 2.6 days) than those predicted by the 1 and 4 cracks models (at 1.95 days in both cases) for series B, see Fig. 4, but this difference is not observed for series A, see Fig. 3. It can be hypothesized that the use of a mechanical model allowing the creation of more initial cracks around the steel rebar would be more realistic and it would lead to a better agreement between the predicted and experimentally observed times of appearance of the first surface crack.

Figs. 5a and 6a show the maximum tensile stress in *Pa* calculated at 23 days through the 1 crack model for series A and B, respectively. Red areas show where cement mortar tensile strength has been exceeded. The observed situation indicates that more cracks will surely appear and that a model with more propagating cracks could better describe the real process. Similar results are obtained using the 4 cracks model. Figs. 7a and 8a show the maximum tensile stress in *Pa* calculated at 23 days through the 8 cracks model for series A and B, respectively. It can be seen that the red areas where the cement mortar tensile strength has been exceeded are smaller, especially in Fig. 8a. That indicates that the 8 cracks model for series B is the one that better describes the real situation and would explain why it better predicts the time of appearance of the first crack, as seen in Fig. 4. It can also be seen that in all cases (Figs. 5a–8a) cement mortar tensile strength is exceeded around the reinforcement contour. According to this, it seems that modeling could be improved allowing the possibility that more than 8 cracks could spread around the reinforcement.

Figs. 5b, 6b, 7b and 8b show the horizontal displacement in *m*, positive to the right, calculated at 23 days through the 1 and 8 cracks models for series A and B. The surface movement due to crack growth can be seen here, as also the mortar displacement in the whole sample

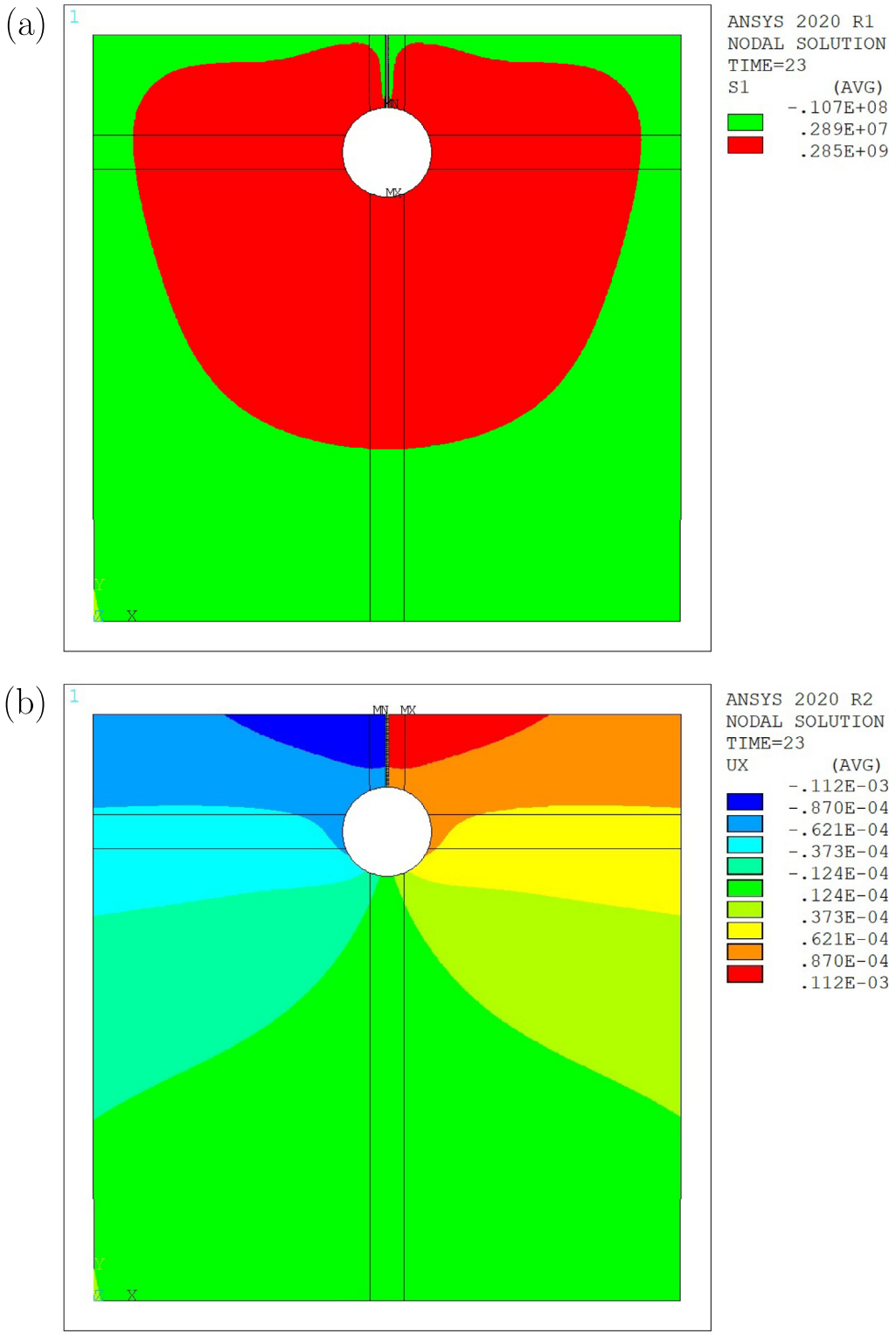

Fig. 5. Maximum tensile stress (S1 in *Pa*, (a)) and horizontal displacement (UX in *m*, (b)) calculated through 1 crack model for series A at 23 days.

can be seen. It is worth noting in Fig. 8b the appearance of two large wedge-shaped volumes between cracks separating (large displacement values) from the rest of the sample. This seems to indicate that the sample will break detaching two big wedge-shaped chunks. Some meshing tests have shown that a non-symmetric meshing can lead to unrealistic non-symmetrical results. Displacement figures like the ones shown in Figs. 5b to 8b are useful to check that the finite element mesh is symmetric enough to assure the symmetry of the results.

Compressive strength f_{cm} is the main parameter affecting the mechanical properties in the used model (see Section 3). A sensitivity analysis on this parameter has been performed. The experimental value $f_{cm} = 29\ MPa$ was used as reference standard, and simulations

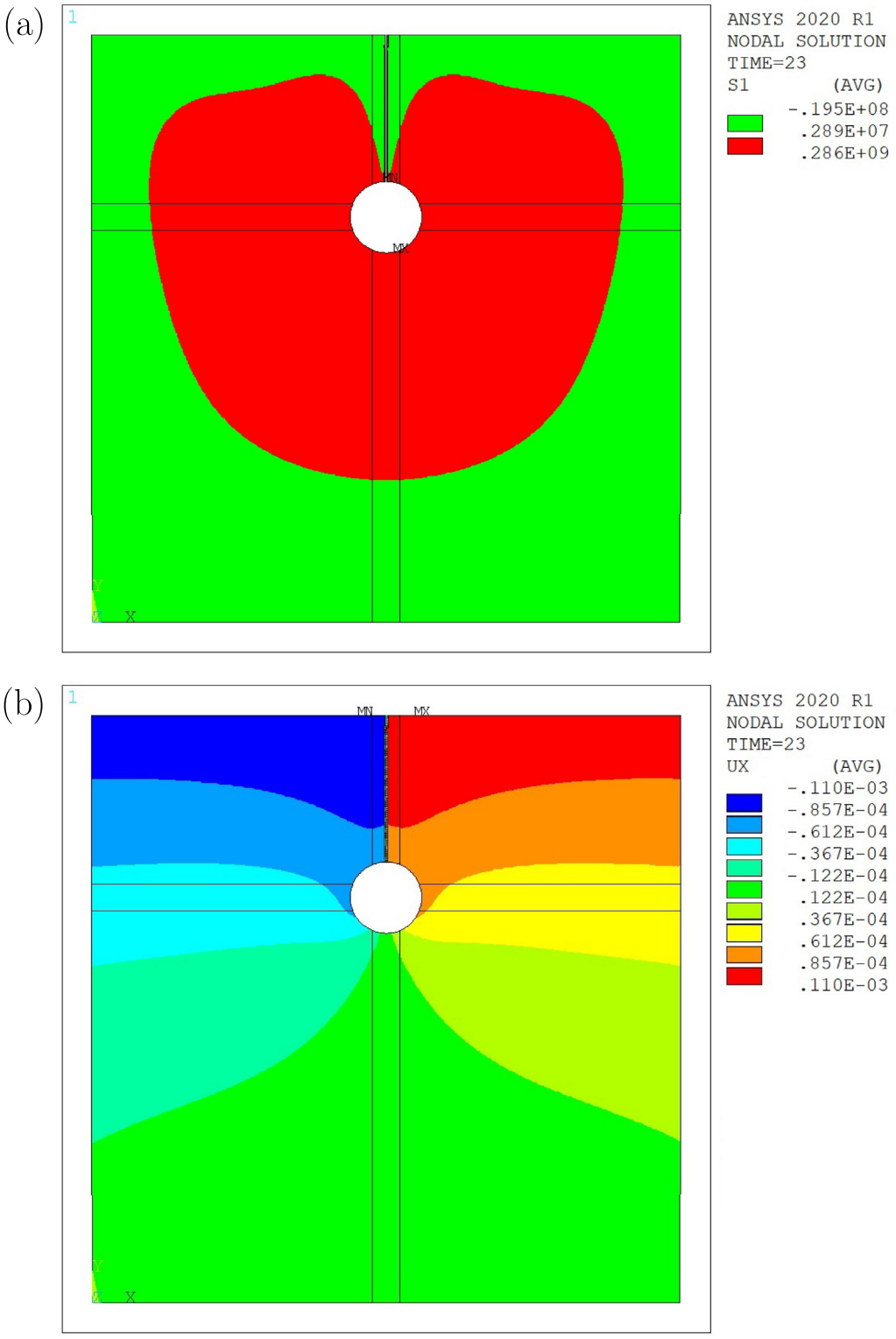

Fig. 6. Maximum tensile stress (S1 in *Pa*, (a)) and horizontal displacement (UX in *m*, (b)) calculated through 1 crack model for series B at 23 days.

with 10% and 20% higher and lower values of f_{cm} where computed. The geometry of series A was considered. The obtained graph of crack width vs. time is shown in Fig. 9. No difference is observed between calculations made with the standard value of f_{cm} and the calculations made with f_{cm} values higher than the standard. For lower values of f_{cm} a different behavior is observed at short times up to approximately 4 days. For longer times the results are similar to the standard. For low compressive strength the model predicts an earlier crack appearance at approximately 0.6 days (compared to approximately 2 days for standard f_{cm} value). Growth would be slower than with the standard value of f_{cm} and crack width would be similar to standard from 4 days onward. Unfortunately our experimental setup would probably not be able to distinguish both situations as the crack width is small (about 30 μm) when both models converge.

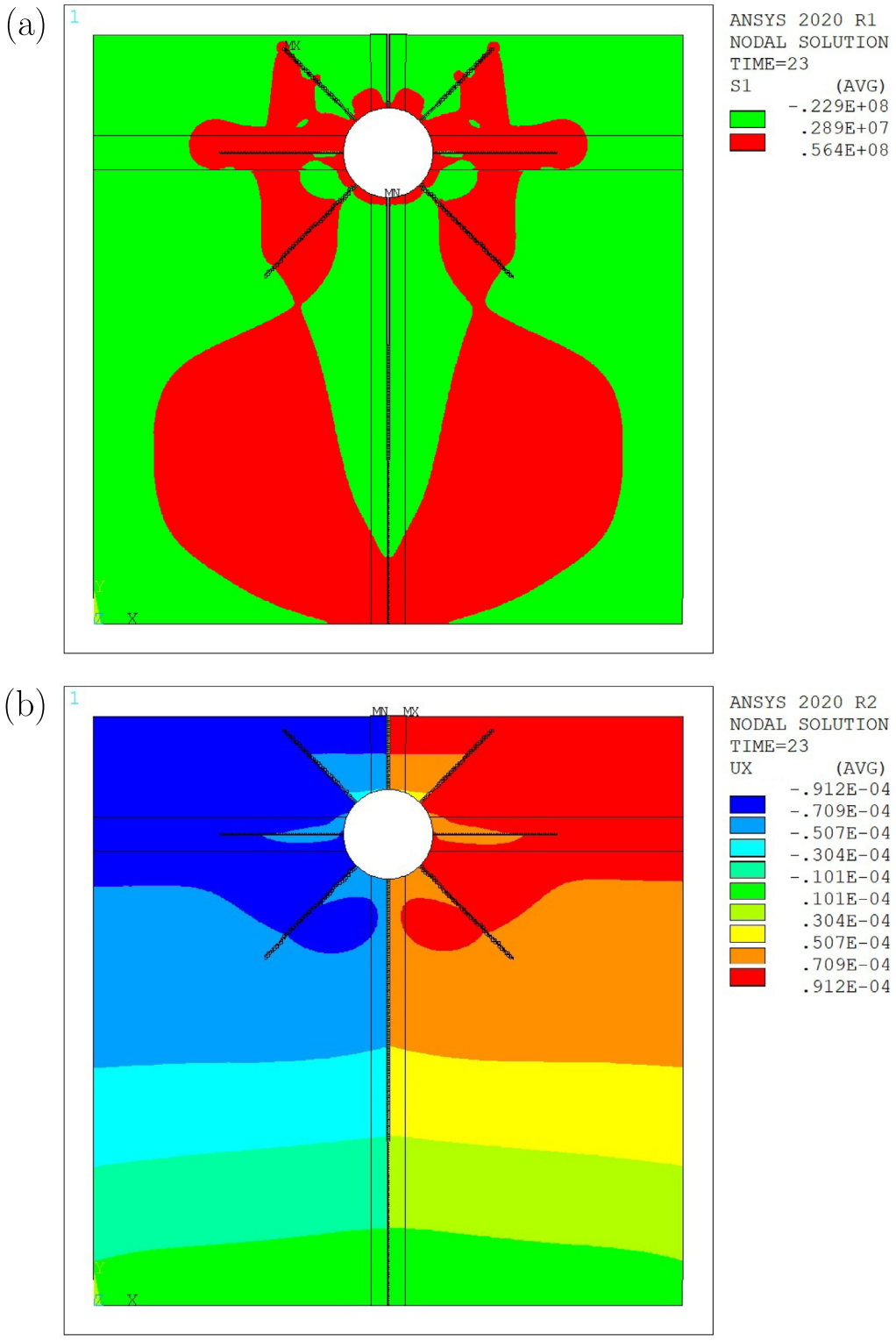

Fig. 7. Maximum tensile stress (S1 in *Pa*, (a)) and horizontal displacement (UX in *m*, (b)) calculated through 8 cracks model for series A at 23 days.

The XFEM-Based Crack Growth Simulation module of Ansys Software can be used for modeling the cracking process of simple reinforced cement mortar specimens due to accelerated corrosion of an embedded steel bar. The consideration of only one main crack, the one first reaching the surface of the specimen, leads to an unacceptable distribution of maximum stresses around the rebar and also in other regions of the cementitious composite. Figs. 5a and 6a depict wide regions showing maximum stresses far higher than the mortar's tensile strength. For a more realistic description of the distribution of the tensile stresses and of the whole cracking process, the model must consider the initiation of several cracks, at least eight, around the rebar perimeter. Obviously, the inclusion in the model of higher number of cracks increases greatly the computation time, convergence difficulties and effort. Regarding the ability to accurately predict the time to

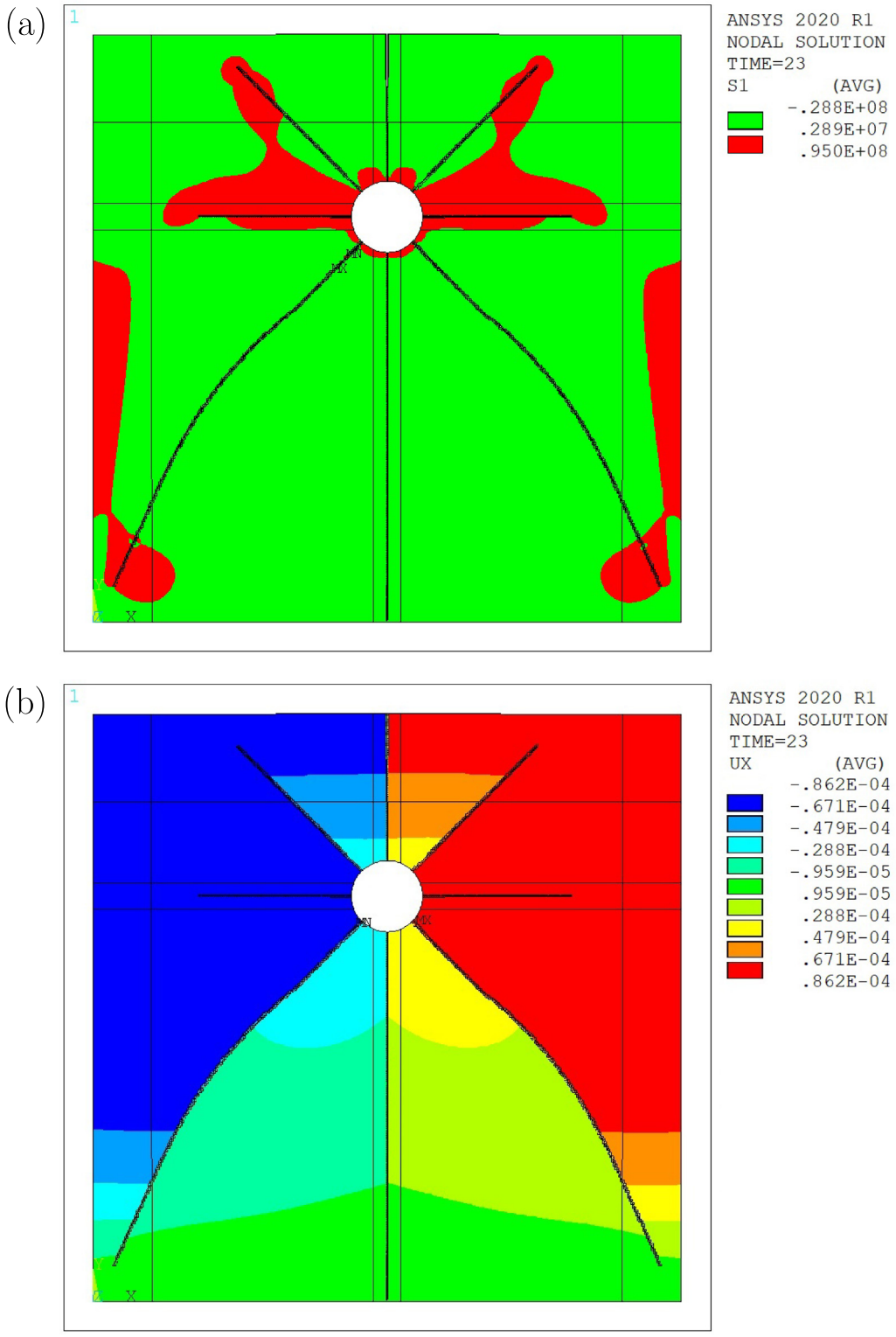

Fig. 8. Maximum tensile stress (S1 in *Pa*, (a)) and horizontal displacement (UX in *m*, (b)) calculated through 8 cracks model for series B at 23 days.

cracking, since the beginning of the accelerated corrosion, the model has led in all cases to shorter times than those observed experimentally, see Figs. 3 and 4. However, it must be considered that in these calculations no allowance has been included for transport of the steel corrosion products away from the rebar, i.e. it has been considered that all the corrosion products remain accumulated as a solid layer around the rebar. This must be considered as a first simple approach to the description of the process. It is thought that the consideration of transport of a portion of the corrosion products away from the rebar could give rise to an improvement of the prediction accuracy regarding the time to cracking, which is one of the main outputs of this kind of modellization.

To sum up, the combined electrochemical and mechanical model has been used reaching an acceptable prediction of the time to appear-

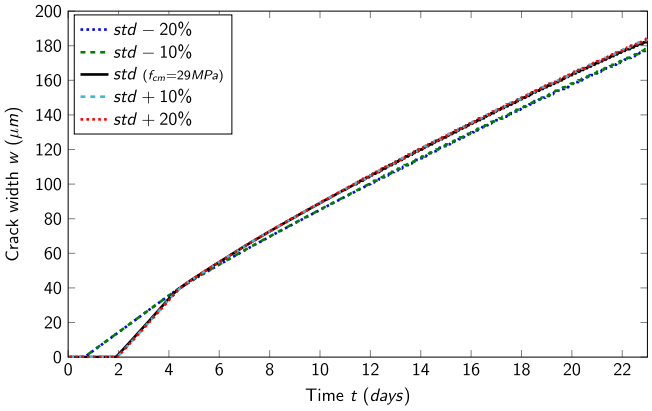

Fig. 9. Sensitivity analysis. Computed crack width vs. time for different values of compressive strength.

ance of the crack on the surface, and the evolution of the crack width over time, during accelerated corrosion tests of reinforced cement mortar specimens. This combined model, which needs only data of a few experimental parameters, and uses only readily accessible standard software, could easily be implemented with other experimental configurations. However, further research taking into account the above mentioned aspects would be desirable.

5. Conclusions

An electrochemical model has been used for describing the inner displacements and strains caused by the accumulation of steel corrosion products around the rebar during electrically accelerated corrosion tests of reinforced cement mortar specimens with simple geometries. Subsequently, a mechanical model using the XFEM-Based Crack Growth Simulation module of Ansys Software, has been implemented to describe the distribution of stresses in the cross-section of the specimens during the corrosion process.

The combined electrochemical and mechanical model has led to predictions of the evolution of crack width over time, which may be considered as in fairly good agreement with experimental data, especially for the specimens with smaller cross section and concrete cover depth. Regarding the ability to accurately predict the time to cracking, since the beginning of the accelerated corrosion, the model has led in all cases to shorter times than those observed experimentally. However, it must be considered that in these calculations no allowance has been included for transport of the steel corrosion products away from the rebar, i.e. it has been considered that all the corrosion products remain accumulated as a solid layer around the rebar.

The calculated distributions of stresses in the cross section of the specimens show that the consideration of only one main crack, the one first reaching the surface of the specimen, leads to an unacceptable distribution of maximum stresses around the rebar and also in other regions of the cementitious composite. There are wide regions showing maximum stresses far higher than the mortar's tensile strength. For a more realistic description of the distribution of the tensile stresses and of the whole cracking process, the model must consider the initiation of several cracks, at least eight, around the rebar perimeter. Obviously, the inclusion in the model of higher number of cracks increases greatly the computation time and effort, and may lead to convergence difficulties.

5.1. Funding

This research was funded by the Spanish Agencia Estatal de Investigación (Grant code BIA2016-80982-R) and by the European Regional Development Fund (Grant code BIA2016-80982-R).

CRediT authorship contribution statement

E.G. Segovia: Conceptualization, Methodology, Software, Writing - original draft, Writing - review & editing. **G. de Vera:** Conceptualization, Methodology, Software, Writing - original draft, Writing - review & editing. **M. Miró:** Investigation, Writing - original draft, Writing - review & editing. **J. Ramis:** Conceptualization, Methodology, Project administration, Funding acquisition, Supervision, Validation. **M.A. Climent:** Conceptualization, Methodology, Project administration, Supervision, Investigation, Validation, Writing - review & editing, Funding acquisition.

Declaration of Competing Interest

The authors declare that they have no known competing financial interests or personal relationships that could have appeared to influence the work reported in this paper.

Acknowledgments

We would like to thank Carmen Andrade for advice on the details of the corrosion testing. We thank also Lafarge-Holcim Spain for providing the cement samples for preparing the reinforced mortar specimens. M.M. acknowledges a pre-doctoral fellowship from the Spanish Ministerio de Educación, Cultura y Deporte (FPU16/04078). The authors would like to dedicate this work to honour Prof. Juan M. Feliu on the occasion of his 70^{th} birthday.

References

[1] ACI, Corrosion of metals in concrete. Detroit (Michigan), 1996..
[2] M.A. Climent, C. Gutiérrez, Proof by uv-visible modulated reflectance spectroscopy of the breakdown by carbonation of the passivating layer on iron in alkaline solution, Surface Science Letters 330 (1995) L651–L656.
[3] C.L. Page, P. Lambert, P.R.W. Vassie, Investigations of reinforcement corrosion. 2. Electrochemical monitoring of steel in chloride-contaminated concrete, Materials and Structures 24 (1991) 351–358.
[4] K. Suda, S. Misra, K. Motohashi, Corrosion products of reinforcing bars embedded in concrete, Corrosion Science 35 (5–8) (1993) 1543–1549.
[5] E. Sola, J. Ozbolt, G. Balabanic, Z.M. Mir, Experimental and numerical study of accelerated corrosion of steel reinforcement in concrete: Transport of corrosion products, Cement and Concrete Research 120 (2019) 119–131.
[6] C. Alonso, C. Andrade, J. Rodríguez, J.M. Díez, Factors controlling cracking of concrete affected by reinforcement corrosion, Materials and Structures 31 (1998) 435–441.
[7] Y. Liu, R.E. Weyers, Modeling the time-to-corrosion cracking in chloride contaminated reinforced concrete structures, ACI Materials Journal 95 (6) (1998) 675–681.
[8] L. Bertolini, B. Elsener, P. Pedeferri, E. Redaelli, R.B. Polder, Corrosion of Steel in Concrete: Prevention, Diagnosis, Repair, John Wiley & Sons, 2013.
[9] T. Uomoto, S. Misra, Behaviour of concrete beams and columns in marine environment when corrosion of reinforcing bars takes place, in: 2nd International Conference on Concrete in Marine Environment, Farmington Hills, MI, 1988, pp. 127–146. ACI SP-109.
[10] E.C.P. d. Hormigón. EHE-08: Instrucción de hormigón estructural: con comentarios de los miembros de la Comisión Permanente del Hormigón. Ministerio de Fomento, Madrid, Spain, fifth ed., 2011..
[11] A. Jamali, U. Angst, B. Adey, B. Elsener, Modeling of corrosion-induced concrete cover cracking: A critical analysis, Construction and Building Materials 42 (2013) 225–237.
[12] C. Andrade, C. Alonso, F.J. Molina, Cover cracking as function of bar corrosion: Part 1 - experimental test, Materials and Structures 26 (1993) 453–464.
[13] S. Muthulingam, B.N. Rao, Non-uniform corrosion states of rebar in concrete under chloride environment, Corrosion Science 93 (2015) 267–282.
[14] X.D. Cheng, Q.Z. Su, F.L. Ma, X.Q. Liu, X.C. Liang, Investigation on crack propagation of concrete cover induced by non-uniform corrosion of multiple rebars, Engineering Fracture Mechanics 201 (2018) 366–384.
[15] D. Qiao, H. Nakamura, Y. Yamamoto, T. Miura, Crack patterns of concrete with a single rebar subjected to non-uniform and localized corrosion, Construction and Building Materials 116 (2016) 366–377.
[16] R.K.L. Su, Y.L. Zhang, A novel elastic-body-rotation model for concrete cover spalling caused by non-uniform corrosion of reinforcement, Construction and Building Materials 213 (5–8) (2019) 549–560.
[17] Y.L. Zhang, R.K.L. Su, Concrete cover delamination model for non-uniform corrosion of reinforcements, Construction and Building Materials 223 (2019) 329–340.

[18] L. Jin, R.B. Zhang, X.L. Du, Y. Li, Investigation on the cracking behavior of concrete cover induced by corner located rebar corrosion, Engineering Failure Analysis 52 (2015) 129–143.
[19] H. Idrissi, A. Limam, Study and characterization by acoustic emission and electrochemical measurements of concrete deterioration caused by reinforcement steel corrosion, NDT&E International 36 (2003) 563–569.
[20] H.L. Ye, N.G. Jin, C.Q. Fu, X.Y. Jin, Rust distribution and corrosion-induced cracking patterns of corner located rebar in concrete cover, Construction and Building Materials 156 (2017) 684–691.
[21] B.Q. Dong, G.Y. Shi, P. Dong, W.J. Ding, X.J. Teng, S.F. Qin, Y.Q. Liu, F. Xing, S.X. Hong, Visualized tracing of rebar corrosion evolution in concrete with x-ray micro-computed tomography method, Cement & Concrete Composites 92 (2018) 102–109.
[22] F. Pedrosa, C. Andrade, Corrosion induced cracking: Effect of different corrosion rates on crack width evolution, Construction and Building Materials 133 (2017) 525–533.
[23] C876 15 ASTM, Standard Test Method for Corrosion Potentials of Uncoated Reinforcing Steel in Concrete, ASTM, Philadelphia, 2009..
[24] R. Rodrigues, S. Gaboreau, J. Gance, I. Ignatiadis, S. Betelu, Reinforced concrete structures: A review of corrosion mechanisms and advances in electrical methods for corrosion monitoring, Construction and Building Materials 121240 (2020).
[25] B. Elsener, C. Andrade, J. Gulikers, R. Polder, M. Raupach, Half-cell potential measurements - potential mapping on reinforced concrete structures, Materials and Structures 36 (261) (2003) 461–471.
[26] R.B. Polder, Test methods for on site measurement of resistivity of concrete - a rilem tc-154 technical recommendation, Construction and Building Materials 15 (2–3) (2001) 125–131.
[27] C. Andrade, J.A. Gonzalez, Quantitative measurement of corrosion rate of reinforcing steels embedded in concrete using polarization resistance measurements, Werkstoffe Und Korrosion-Materials and Corrosion 29 (8) (1978) 515–519.
[28] C. Andrade, C. Alonso, Corrosion rate monitoring in the laboratory and on-site, Construction and Building Materials 10 (5) (1996) 315–328.
[29] S. Sharma, A. Mukherjee, Monitoring corrosion in oxide and chloride environments using ultrasonic guided waves, Journal of Materials in Civil Engineering 23 (2) (2011) 207–211.
[30] S. Sharma, A. Mukherjee, Longitudinal guided waves for monitoring chloride corrosion in reinforcing bars in concrete, Structural Health Monitoring-an International Journal 9 (6) (2010) 555–567.
[31] A.A. Shah, Y. Ribakov, Non-destructive evaluation of concrete in damaged and undamaged states, Materials & Design 30 (9) (2009) 3504–3511.
[32] A. Zaki, H.K. Chai, D.G. Aggelis, N. Alver, Non-destructive evaluation for corrosion monitoring in concrete: A review and capability of acoustic emission technique, Sensors 15 (8) (2015) 19069–19101.
[33] L. Calabrese, G. Campanella, E. Proverbio, Identification of corrosion mechanisms by univariate and multivariate statistical analysis during long term acoustic emission monitoring on a prestressed concrete beam, Corrosion Science 73 (2013) 161–171.
[34] M. Ohtsu, T. Shiotani, M. Shigeishi, T. Kamada, S. Yuyama, T. Watanabe, T. Suzuki, J.G.M. van Mier, T. Vogel, C. Grosse, R. Helmerich, M.C. Forde, A. Moczko, D. Breysse, S.A. Ivanovich, A. Sajna, D. Aggelis, G. Lacidogna, R.T. Comm, Recommendation of RILEM TC 212-ACD: acoustic emission and related nde techniques for crack detection and damage evaluation in concrete measurement method for acoustic emission signals in concrete, Materials and Structures 43 (9) (2010) 1177–1181.
[35] M. Liang, P. Su, Detection of the corrosion damage of rebar in concrete using impact-echo method, Cement and Concrete Research (2001) 1427–1436.
[36] A.A. Shah, Y. Ribakov, S. Hirose, Nondestructive evaluation of damaged concrete using nonlinear ultrasonics, Materials & Design 30 (3) (2009) 775–782.
[37] A.A. Shah, Y. Ribakov, Non-linear ultrasonic evaluation of damaged concrete based on higher order harmonic generation, Materials & Design 30 (10) (2009) 4095–4102.
[38] K.Y. Jhang, Nonlinear ultrasonic techniques for non-destructive assessment of micro damage in material: A review, International Journal of Precision Engineering and Manufacturing 10 (1) (2009) 123–135.
[39] S. Guzmán, J.C. Gálvez, J.M. Sancho, Cover cracking of reinforced concrete due to rebar corrosion induced by chloride penetration, Cement and Concrete Research 41 (2011) 893–902.
[40] L. Chernin, D.V. Val, K.Y. Volokh, Analytical modelling of concrete cover cracking caused by corrosion of reinforcement, Materials and Structures 43 (2010) 543–556.
[41] S. Guzmán, J.C. Gálvez, Modelling of concrete cover cracking due to non-uniform corrosion of reinforcing steel, Construction and Building Materials 155 (2017) 1063–1071.
[42] J. Zhang, X. Ling, Z. Guan, Finite element modeling of concrete cover crack propagation due to non-uniform corrosion of reinforcement, Construction and Building Materials 132 (2017) 487–499.
[43] T.Y. Pan, Y. Lu, Stochastic modeling of reinforced concrete cracking due to nonuniform corrosion: Fem-based cross-scale analysis, Journal of Materials in Civil Engineering 24 (6) (2012) 698–706.
[44] Y.X. Zhao, B.Y. Hu, J. Yu, W.L. Jin, Non-uniform distribution of rust layer around steel bar in concrete, Corrosion Science 53 (12) (2011) 4300–4308.
[45] Y.X. Zhao, X.W. Zhang, H.J. Ding, W.L. Jin, Non-uniform distribution of a corrosion layer at a steel/concrete interface described by a gaussian model, Corrosion Science 112 (2016) 1–12.
[46] X. Xi, S.T. Yang, C.Q. Li, A non-uniform corrosion model and meso-scale fracture modelling of concrete, Cement and Concrete Research 108 (2018) 87–102.
[47] M.A. Climent, M. Miró, J. Carbajo, P. Poveda, G. de Vera, J. Ramis, Use of non-linear ultrasonic techniques to detect cracks due to steel corrosion in reinforced concrete structure, Materials 12 (2019) 819.
[48] M.A. Climent-Llorca, M. Miro-Oca, P. Poveda-Martinez, J. Ramis-Soriano, Use of higher-harmonic and intermodulation generation of ultrasonic waves to detecting cracks due to steel corrosion in reinforced cement mortar, International Journal of Concrete Structures and Materials 14 (1) (2020) 17.
[49] G. de Vera, M. Miró, E.G. Segovia, P. Poveda, M.A. Climent, Rebar shape time-evolution during a reinforced concrete corrosion test: an electrochemical model, Applied Sciences 9 (15) (2019) 3061.
[50] ANSYS, Inc. ANSYSAcademic Research Mechanical, Release 2019 R3, Help System..
[51] T. Belytschko, T. Black, Elastic crack growth in finite elements with minimal remeshing, International Journal for Numerical Methods in Engineering 45 (1999) 601–620.
[52] Asociación Española de Normalización y Certificación, Madrid, Spain. UNE-EN 197-1 Cemento. Parte 1: Composición, Especificaciones y Criterios de Conformidad de los Cementos Comunes (Cement. Part 1: Composition, Specifications and Conformity Criteria for Common Cements), 2011. In Spanish, equivalent to the European Standard EN 197-1..
[53] M.A. Climent, G. de Vera, E. Viqueira, M.M. López, Generalization of the possibility of eliminating the filtration step in the determination of acid-soluble chloride content in cement and concrete by potentiometric titration, Cement and Concrete Research 34 (2004) 2291–2295.
[54] Asociación Española de Normalización y Certificación, Madrid, Spain. UNE-EN 196-1 Methods of testing cement - Part 1: Determination of strength, 2018..
[55] ASTM C. 642-97, Standard Test Method for Density, Absorption, and Voids in Hardened Concrete, ASTM, West Conshohocken, PA..
[56] ASTM G 1-90, Standard practice for preparing, cleaning and evaluating corrosion test specimens, ASTM, West Conshohocken, PA..
[57] F.J. Molina, C. Alonso, C. Andrade, Cover cracking as function of rebar corrosion: Part 2 - numerical model, Materials and Structures 26 (1993) 532–548.
[58] J. Melenk, I. Babuska, The partition of unity finite element method: Basic theory and applications, Computer Methods in Applied Mechanics and Engineering 39 (1996) 298–314.
[59] J.J.C. Remmers, R. de Borst, A. Needleman, The simulation of dynamic crack propagation using the cohesive segments method, Journal of the Mechanics and Physics of Solids 56 (2008) 70–92.
[60] J.H. Song, P.M.A. Areias, T. Belytschko, A method for dynamic crack and shear band propagation with phantom nodes, Journal for Numerical Methods in Engineering 67 (2006) 868–893.
[61] Q. Duan, J.H. Song, T. Menouillard, T. Belytschko, Element-local level-set method for three-dimensional dynamic crack growth, International Journal for Numerical Methods in Engineering 80 (2009) 1520–1543.
[62] F. Erdogan, G.C. Sih, On the crack extension in plates under plane loading and transverse shear, ASME Journal of Basic Engineering 85 (1963) 519–527.
[63] M. Ortiz, A. Pandolfi, Finite-deformation irreversible cohesive elements for three-dimensional crack- propagation analysis, International Journal for Numerical Methods in Engineering 44 (1999) 1267–1282.
[64] CEB/FIP Model Code 1990, Textbook on Behaviour, Design and Performance, vol. 1: Introduction – Design Process – Materials, 1990..
[65] Herry Suryadi Djayaprabha, Ta-Peng Chang, Jeng-Ywan Shih, Comparison study of dynamic elastic moduli of cement mortar and no-cement slag based cementitious mortar activated with calcined dolomite with impulse excitation technique, MATEC Web Conf. 186 (2018) 02004.